

THE HADS STAR CSS_J102714.3+205943: A COMPONENT OF A BINARY SYSTEM WITH AN ELLIPTIC ORBIT?

PYATNYTSKY, MAKSYM YU.¹ AND ANDRONOV, IVAN L.²

- 1) Private Observatory "Osokorky", PO Box 27, 02132 Kyiv, Ukraine, pmak@osokorky-observatory.com
- 2) Department of Mathematics, Physics and Astronomy, Odesa National Maritime University, Mechnikova 34, 65029 Odesa, Ukraine

Abstract: We analyzed period changes of the high-amplitude Delta Scuti variable star CSS_J102714.3+205943 for about 20 years, utilizing data from the automated sky surveys along with our own observations. With the help of the $O - C$ diagram, we found that the period decreased noticeably between JD2454800 and JD2457300. A possible cause of the change could be intrinsic processes in the star. However, the observed behavior of the $O - C$ diagram can also be explained by the light-time effect if the star is a component of a binary system. Times of maxima for the star, derived from the surveys and our observations, are listed.

1 Introduction

As defined in (Baglin et al., 1973), Delta Scuti stars are short-period (from 0.02 to 0.2 days) pulsating variables of spectral types between A2V and F0V. They occupy a place in the Hertzsprung-Russell diagram where the extension of the Cepheid instability strip crosses the main sequence (Breger, 2000a; Handler, 2009). A more recent definition of the Delta Scuti variability type (DSCT) from the International Variable Star Index (VSX) (Watson, Henden & Price, 2006) is broader and includes "pulsating variables of spectral types A0-F5 III-V displaying light amplitudes from 0.003 to 0.9 magnitudes in V " ¹, with periods from 0.01 to 0.2 days. The subset of Delta Scuti stars with a relatively high range of pulsations above $0.^m3$ in V (Breger, 2000b; Handler, 2009) ($0.^m15$ according to VSX) are called high-amplitude DSCT stars (HADS).

Delta Scuti stars are important for asteroseismology (Breger, 2000a). Also, because they have their own period-luminosity relationship (McNamara, 1997, 2011; Ziaali et al., 2019), these stars can be used as 'standard candles' for measuring distances (McNamara et al., 2000).

In the current research, we investigated the period change of the poorly studied HADS star CSS_J102714.3+205943 = GSC 01426-00590 = ZTF J102714.30+205943.4 = TIC 171599792. According to VSX, the period of the star is 0.0684195 days, the variability range is $0.^m442$ in the g band. Using the estimated star's luminosity ($9.6L_{\odot}$) and effective temperature ($7505K$) from (Gaia Collaboration, 2022), we can see that the star is indeed located in the area of the HR diagram where the instability strip crosses the main sequence (Fig. 1).

¹<https://www.aavso.org/vsx/index.php?view=about.vartypes>

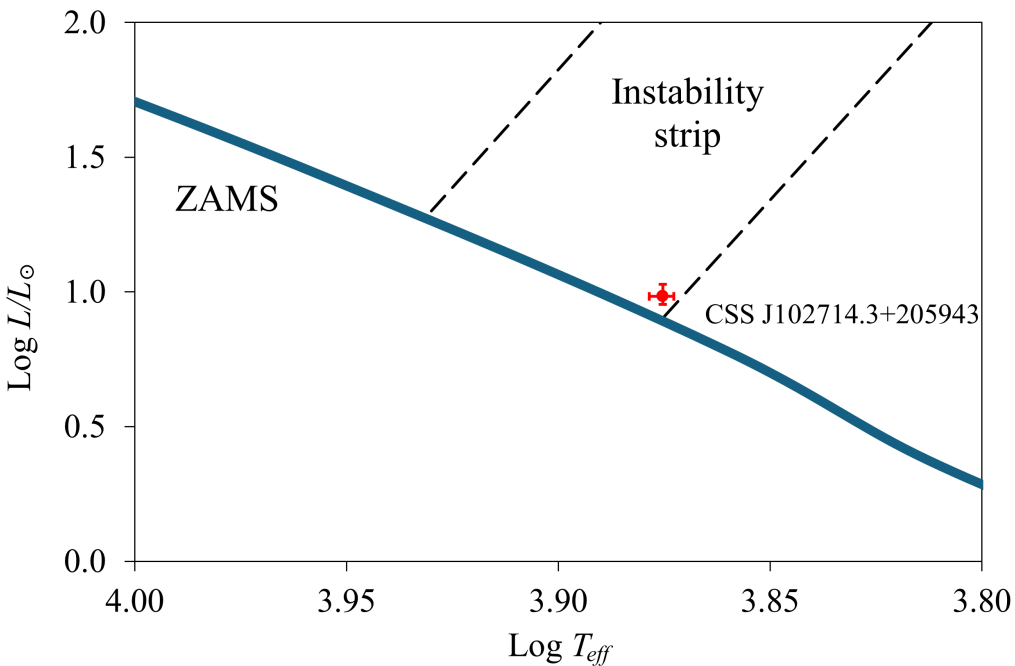


Figure 1: The Hertzsprung–Russell diagram with the Zero Age Main Sequence (ZAMS) and the instability strip. The red dot with error bars indicates the location of CSS_J102714.3+205943 according to the Gaia DR3 catalogue.

2 Observation and data reduction

We analyzed our observations and data from automatic surveys. For primary data manipulation, such as converting between different survey formats, visually inspecting, and removing outliers, we utilized the VStar software (Benn, 2012; Benn et al., 2024).

2.1 Our observations

The observation of CSS_J102714.3+205943 was carried out in February 2022 from Kyiv, Ukraine, for three nights. We used a 150mm Newtonian telescope with a focal length of 750mm, equipped with the cooled monochrome CMOS camera ZWO ASI183MM Pro and the V photometric filter.

The light frames were treated with a standard procedure using dark, flat, and dark-flat calibration frames. The calibration frames were taken every observation night immediately after the observing session. To take the flat frames, we used a white paper screen placed about 2 meters from the telescope illuminated by an LED lamp.

A sample image with the object and the comparison stars is shown in Fig. 2. These stars were selected according to the AAVSO recommended sequence². Magnitudes of the stars were taken from the APASS DR10 survey (Henden et al., 2018). Detailed information about the comparison stars is given in Tab. 1.

²<https://apps.aavso.org/vsp/photometry/?chartid=X38581CXQ>

Table 1: Comparison and check stars.

ID	Type	RA (2000) [h:m:s]	DEC (2000) [$^{\circ}$ ' "]	V [mag]
TYC 1426-1013-1	Comp	10:26:52.9	+20:40:29.3	10.784(69)
TYC 1426-979-1	Check	10:25:39.6	+20:41:52.8	10.999(69)

The differential aperture photometry was conducted using the AstroImageJ software (Collins et al., 2017).

A phase plot of the resulting light curve is shown in Fig. 3.

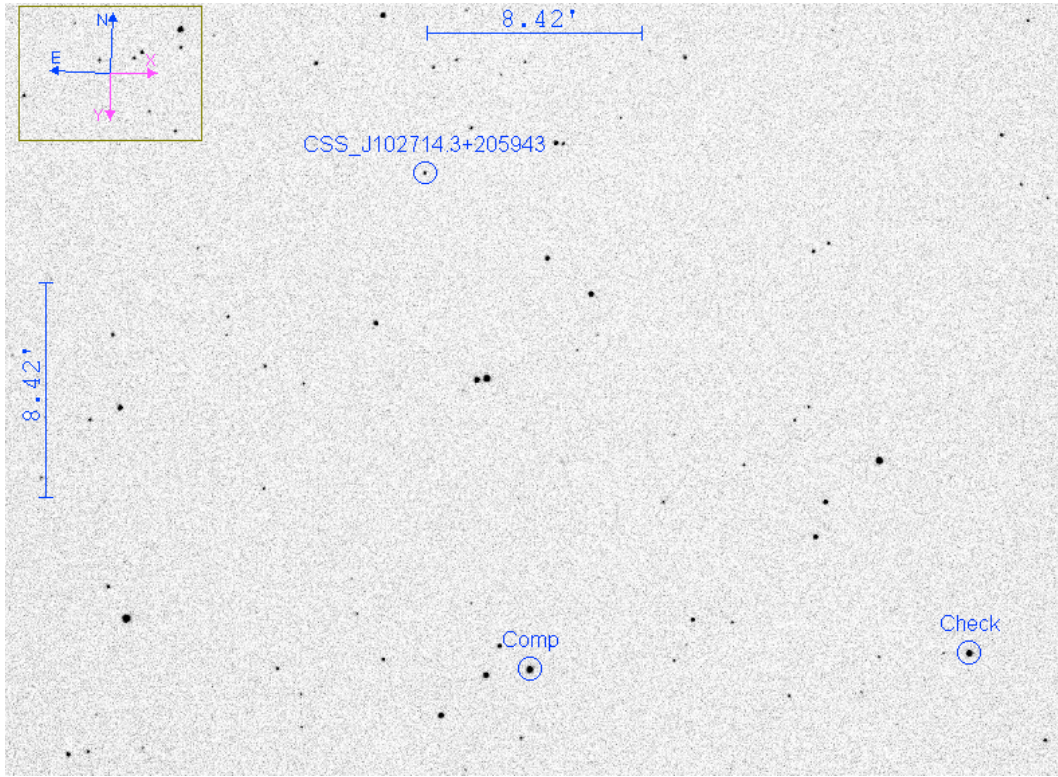


Figure 2: A sample image showing the FOV with the object and the comparison stars.

2.2 Data from the TESS survey

Another source of the continuous light curve was the TESS survey (Ricker et al., 2014).

Checking the MAST Portal³ revealed that there were no ready-to-use light curves available. However, there were TESS Full Frame Images (FFI) data for TESS sectors 45, 46, 48, and 72. The exposure lengths for sectors 45, 46, and 48 were too long (475 seconds) for the star with such a short period. The exposure for sector 72 was 158 seconds (with 200 seconds between frames), which is appropriate.

³<https://mast.stsci.edu/portal/Mashup/Clients/Mast/Portal.html>

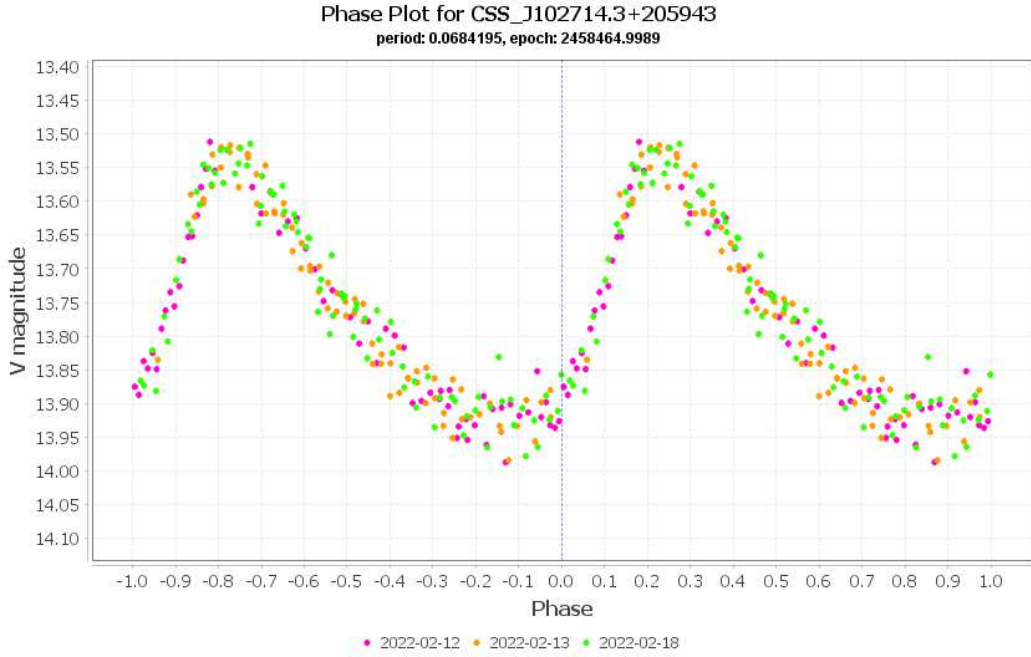


Figure 3: Phase plot of our observations over three nights (see legend). The period and initial epoch are taken from VSX for November 2024.

We used the 'Lightkurve' Python package (Lightkurve Collaboration, 2018) to generate the TESS light curve.

For sector 72, we extracted a set of target pixel images (TPI) of the star's vicinity of size 13×13 pixels, corresponding to 4.55×4.55 arcminutes. Then, we created a measurement aperture with the 'create_threshold_mask' function, taking pixels with a median flux that is greater than 7 times the standard deviation above the overall median. A sample target image with the aperture mask is shown in Fig. 4a. To estimate the background level, we used the background aperture shown in Fig. 4b. For each TPI, we calculated the star's flux inside the measurement aperture, subtracted the estimated background level, and thus obtained the light curve. Then, we visually inspected the light curve and rejected parts with apparent parasitic flux. Using the TESS magnitude of the star from the TESS Input Catalog - v8.0 (Stassun et al., 2019) (13^m579) as the reference mean magnitude, we converted the fluxes to magnitudes, obtaining the final light curve. A phase plot of the TESS light curve is shown in Fig. 5.

2.3 Data from other surveys

For our analysis, we also used data from other surveys, namely, CRTS (Drake et al., 2009), SuperWASP (Butters et al., 2010), ASAS-SN (Kochanek et al., 2017), and ZTF (Masci et al., 2019).

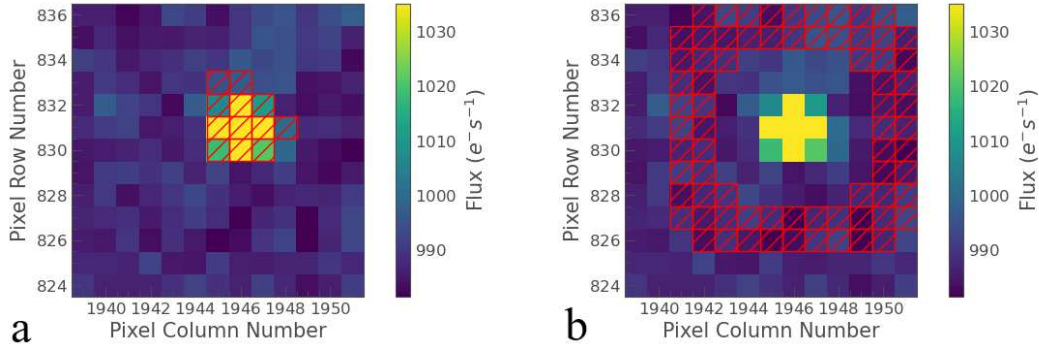


Figure 4: Apertures used for calculating the star's flux from TESS target pixel images: (a) the measurement aperture; (b) the aperture used for estimating the background signal level.

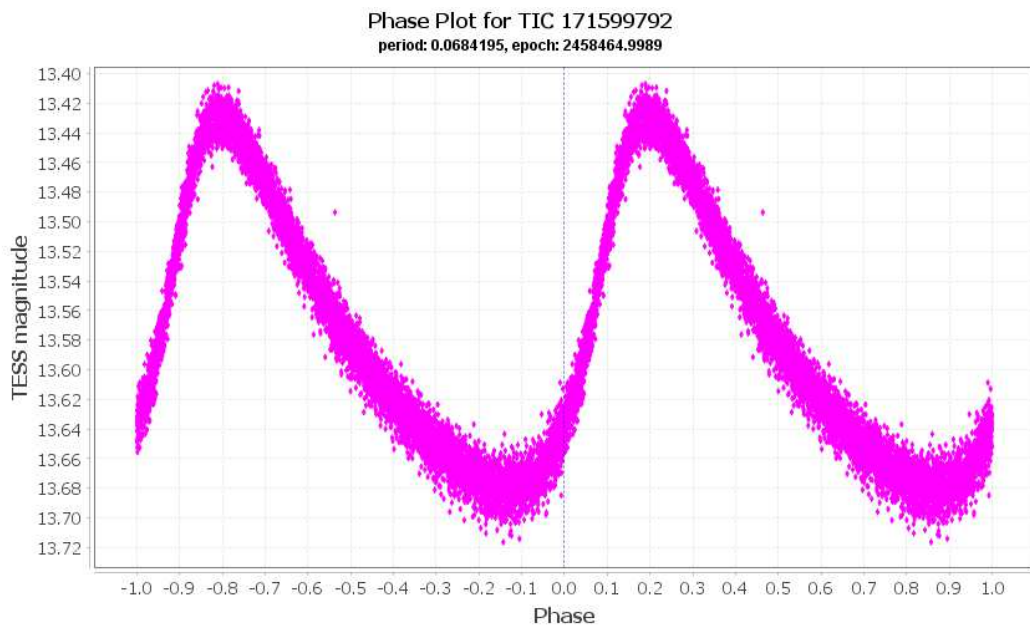


Figure 5: TESS phase plot. The period and initial epoch are taken from VSX for November 2024.

3 Data analysis

When we tried to combine all the data, we found that it was impossible to choose a single period for all observations. Therefore, we assumed that the period changes over time. A commonly used method for investigating period changes is the $O - C$ diagram. To build the diagram, we need precise times of maxima (TOMs).

To derive TOMs from the data, we first built a model light curve based on our observations in the V filter, approximating it with trigonometric polynomials. We used the approach described in (Andronov, 1994, 2020) to determine the statistically optimal approximation, which corresponds to the minimal r.m.s. error of the approximations. The following formula defines the optimal approximation:

$$\sigma_m^2[x_C] = \frac{m}{n(n-m)} \sum_{k=1}^n (x_k - x_{Ck})^2 \quad (1)$$

where n is the number of observations, m is the number of parameters, x_k is a k -th observation, x_{Ck} is a k -th calculated (model) point. The number of parameters m is equal to $2s + 2$, where s is the degree of the polynomial (the number of harmonics, including the primary frequency). Another free parameter is the constant level, and an additional one comes from adjusting the primary frequency.

With this approach, utilizing the MCV software (Andronov & Baklanov, 2004; Andronov, 2020), we determined that, besides the main frequency $f_0 = 1/P_0$ (where $P_0 = 0.0684223(33)$ days), we need the second harmonic ($2 \cdot f_0$) and the third harmonic ($3 \cdot f_0$) to adequately approximate the observations, i.e. the $\sigma_m^2[x_C]$ value minimizes for $s = 3$.

The resulting light curve model is shown in Fig. 6. We used the upper part of the model (from the top to half of the maximum) to fit the observed light curve near the maxima, thereby finding the TOMs. We successfully utilized this approach previously for another HADS star (Pyatnytskyy, 2021; Pyatnytskyy & Andronov, 2024).

We used this model for our observations and data from the surveys except for TESS. Given that the survey data are sparse, we folded the survey data over a long period of time before determining the times of maxima (see Tab. 3, column "Half of the folding interval").

We built a separate model for TESS data due to the smaller variability range in the TESS band and the somewhat different curve shape. In this case, we used six harmonics (including the primary frequency) for the approximation. We chose this number of harmonics based on the periodogram (created with VStar) of the TESS data, see Fig. 7.

We found no additional frequencies in the TESS light curve except for the primary one and its harmonics. This suggests that the star is a radial pulsator with a single pulsation mode. This is not unexpected, because although Delta Scuti stars, in general, may exhibit many superimposed pulsation modes (Breger, 2000b), there is evidence that most HADS stars pulsate in a single mode (Xue et al., 2023).

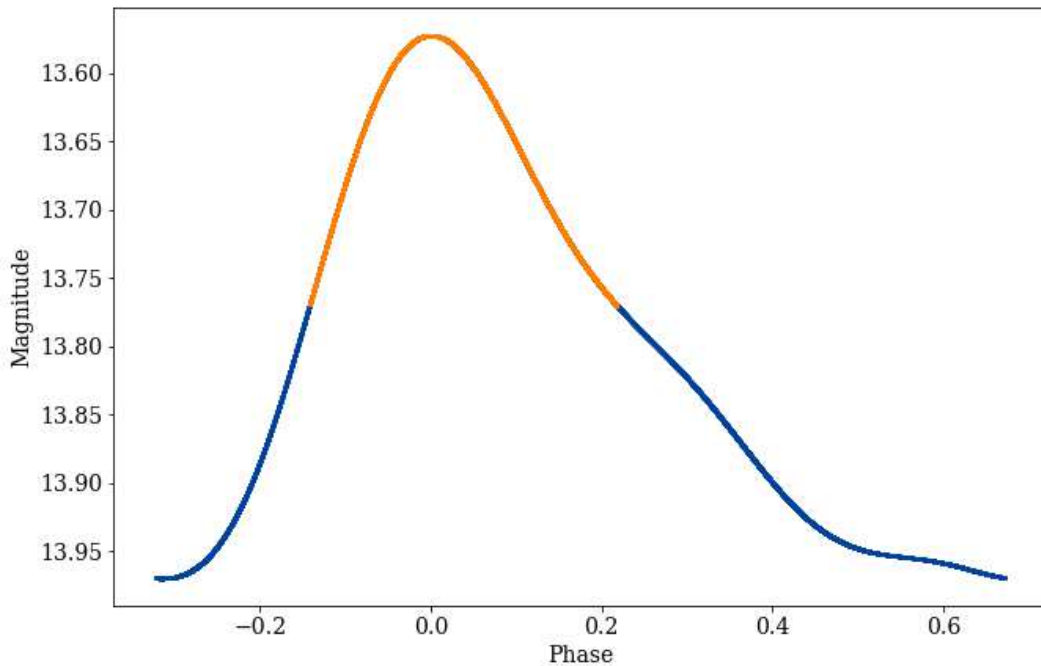


Figure 6: The light curve model for our observations was built using a trigonometric polynomial of the third order. The upper part of the model (light colored) was used for the approximation of TOMs.

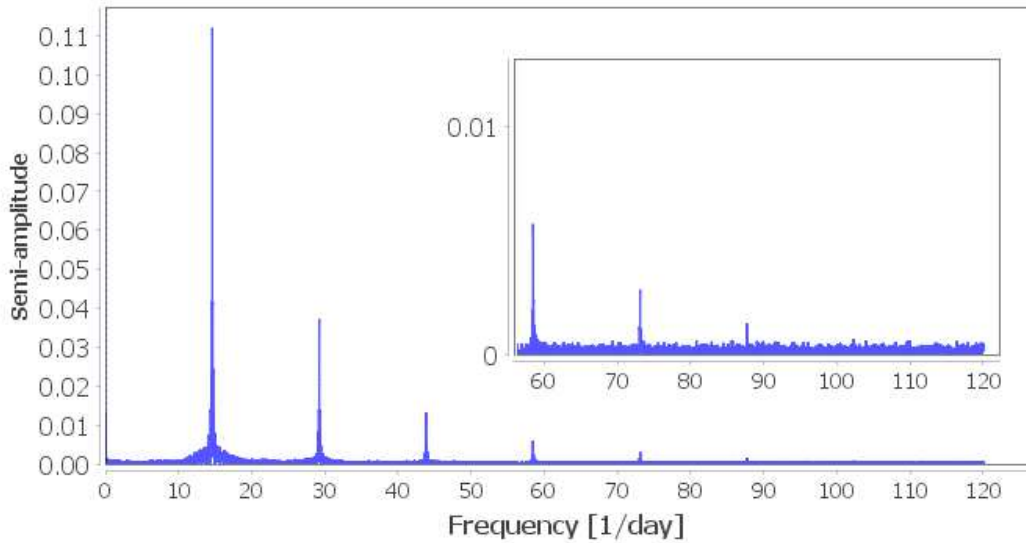


Figure 7: Periodogram of the TESS data.

4 Results

Tab. 3 lists TOMs derived from all the data.

Having determined the TOMs, we built the $O - C$ diagram, as shown in Fig. 8. The diagram corresponds to the following ephemeris:

$$T_{\max}[BJD_{TDB}] = 2459623.42653(3) + 0.068419093(3)E \quad (2)$$

where T_{\max} is the time of a maximum for a cycle number E .

The period in Eq. 2 corresponds to the horizontal flat part of the $O - C$ diagram that starts from $JD \approx 2457300$. This value comes from the approximation using the Asymptotic Parabola (AP) method (Andrych, Andronov, Chinarova & Marsakova, 2015) realized in the MAVKA software (Andrych, Andronov & Chinarova, 2020)⁴.

From the AP approximation, the ascending straight branch of the $O - C$ diagram ends at $JD \approx 2454800$, and the horizontal flat part starts at the previously mentioned value of $JD \approx 2457300$, with a smooth transition between these points. With this interpretation of the $O - C$ diagram, we can state that the star's period decreases from a constant value of $0.068419686(11)$ to $0.068419093(3) d^{-1}$.

Similar period changes have already been observed in other stars of the HADS type (Laney, Joner & Rodriguez, 2003; Axelsen & Napier-Munn, 2020). Their nature, however, is still unclear.

Fig. 9 demonstrates the phased light curve for $JD > 2457300$, which includes datasets in the V filter, i.e., our observations and a part of ASAS-SN data. We also added available photometric data from the Gaia DR3 release (Gaia Collaboration, 2023) to this plot. There are only 29 Gaia DR3 observations in total (each in the G , BP , and RP filters), and only 20 of them since JD2457300 to date, so we did not use them while creating the $O - C$ diagram. Nevertheless, the Gaia DR3 data are in good agreement with other observations. An average Gaia DR3 V magnitude is somewhat dimmer than the one from our observations and ASAS-SN data by $\approx 0.^m03$. This can be due to uncertainties in the transformation of the G , BP , and RP values to V . See the corresponding relationship in the 'Photometric relationships with other photometric systems' section here⁵. From the phase plot, we derived the previously unknown variability range in the V filter and the light curve rise duration time from minimum to maximum magnitude, which characterizes the light curve's asymmetry (see Tab. 2).

However, another interpretation of this bent $O - C$ diagram could be considered. If the star is a component of a binary system, the light-time effect could cause the apparent period changes (Sterken, 2005). With this assumption, the observed deviations in the times of maxima are caused by the star's shift along the line of sight. If a hypothetical second body orbits around the common center of mass, the observed star also moves in an elliptical orbit around the center of mass.

Using the MCV software, we approximated the $O - C$ curve with a second-order trigonometric polynomial with a linear trend. This gave us a starting point for further approximation. Then, we used a combination of manual fitting of the model's parameters

⁴<https://uavso.org.ua/mavka/>

⁵<https://gea.esac.esa.int/archive/documentation/GDR2/>

Table 2: Light curve parameters in the V filter for $JD > 2457300$.

Parameter	Value
Magnitude at minimum	13.92
Magnitude at maximum	13.52
Period [d]	0.068419093
Initial epoch [BJD_{TDB}]	2459623.4265
Rise duration [%]	32

and approximation with the OCFit package (Gajdoš & Parimucha, 2019; Gajdoš, 2023). The interval of the observations is too short and does not cover a single complete orbit. Therefore, for now, we intend to show only the possibility of this interpretation without expecting a precise result.

Fig. 10 shows the result of the modeling. We ended up with the following parameters of the model: rotation period is 32.3*yrs*, the value of $a \sin i$ is 1.45*a.u.* (where a is the orbit's semi-major axis, i is the orbit's inclination), orbit's eccentricity is 0.41, and argument of pericenter is 20°. Further observations over several dozen years are required to prove our interpretation.

If this interpretation is valid, we can estimate the lower limit of the second body's mass. Given that the mass of the observed HADS star CSS_J102714.3+205943 is $1.66M_\odot$ (Gaia Collaboration, 2022), the estimated mass of the second body is $\gtrsim 0.2M_\odot$. So, the second body is likely a red dwarf.

5 Conclusions

We found a period change in the HADS star CSS_J102714.3+205943, which occurred between JD2454800 and JD2457300. The observed change in the period could be caused by intrinsic processes. However, a more straightforward interpretation is possible if we assume that the star is a component of a binary system. If this assumption is valid, the apparent change in the period is caused by a light-time effect. The second component of the binary is likely a red dwarf with a lower mass limit of about $0.2M_\odot$. Further long-term observations are necessary to prove this assumption.

Acknowledgements: This paper includes results derived from data collected by the TESS mission. Funding for the TESS mission is provided by the NASA's Science Mission Directorate.

This work makes use of observations obtained with the Samuel Oschin Telescope 48-inch and the 60-inch Telescope at the Palomar Observatory as part of the Zwicky Transient Facility project. ZTF is supported by the National Science Foundation under Grant No. AST-2034437 and a collaboration including Caltech, IPAC, the Weizmann Institute for Science, the Oskar Klein Center at Stockholm University, the University of Maryland, Deutsches Elektronen-Synchrotron and Humboldt University, the TANGO Consortium of Taiwan, the University of Wisconsin at Milwaukee, Trinity College Dublin, Lawrence Livermore National Laboratories, and IN2P3, France. Operations are conducted by COO, IPAC, and UW. We thank the Las Cumbres Observatory and its staff for their continuing support of the ASAS-SN project.

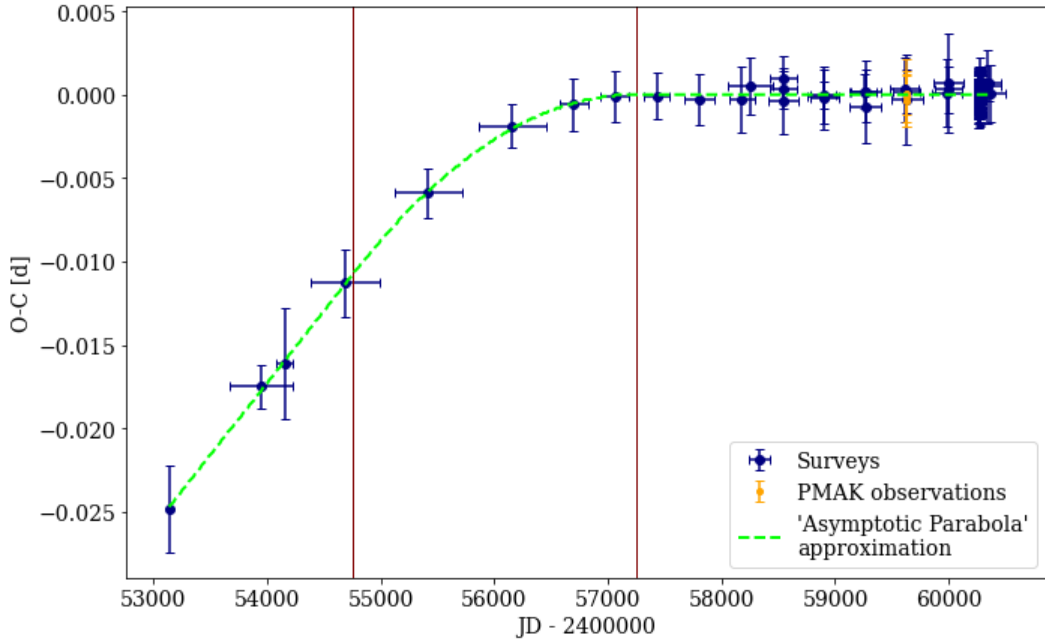


Figure 8: $O-C$ diagram corresponding to Eq. 2. Our observations are labeled as 'PMAK'. Horizontal error bars show folding intervals for the data from the surveys. Vertical lines denote the AP approximation's parabolic part's start and end.

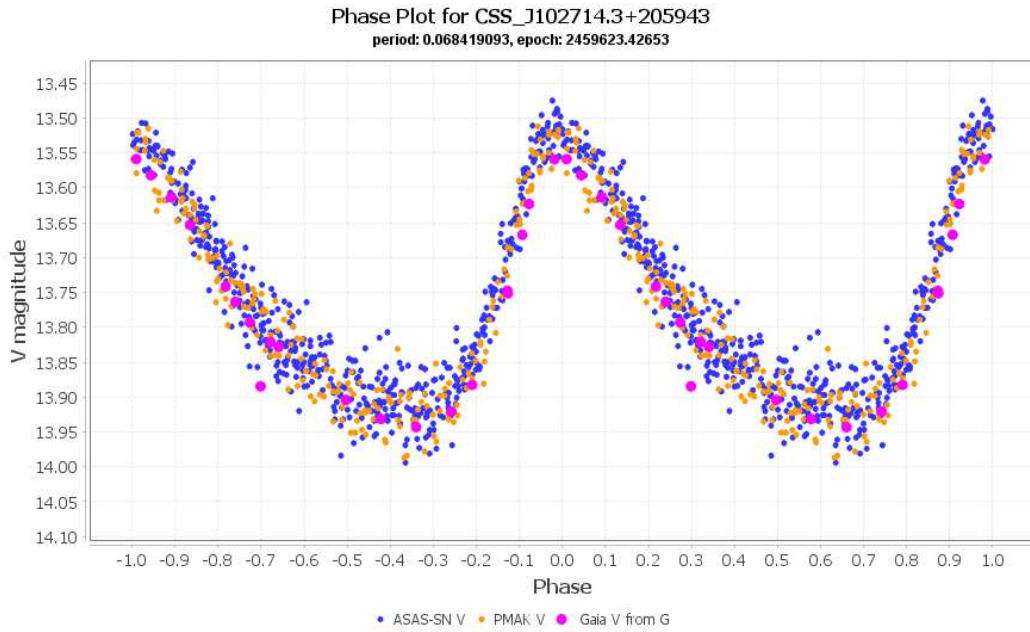


Figure 9: Phase plot with our observations (PMAK), ASAS-SN data in the V filter, and Gaia DR3 data transformed to the V band. The ASAS-SN and Gaia DR3 data are for $JD > 2457300$. The period and initial epoch are from Eq. 2.

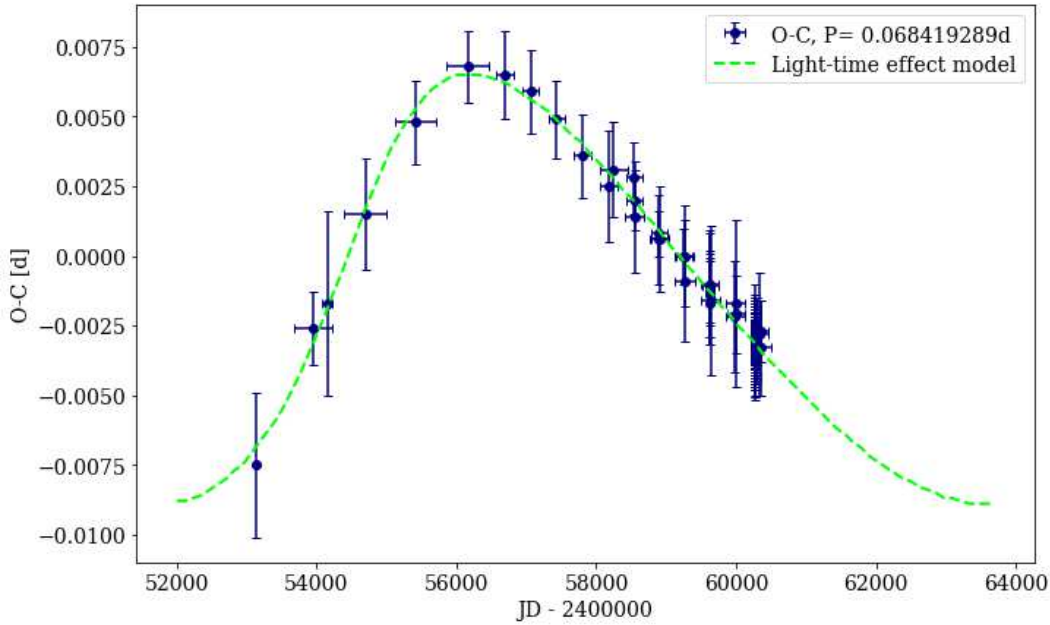


Figure 10: Modified $O - C$ diagram with the light-time effect model.

This paper makes use of data from the DR1 of the WASP data (Butters et al., 2010) as provided by the WASP consortium, and computational resources supplied by the project "e-Infrastruktura CZ" (e-INFRA CZ LM2018140) supported by the Ministry of Education, Youth and Sports of the Czech Republic. We make use of the data from the CSS survey, which is funded by the National Aeronautics and Space Administration under Grant No. NNG05GF22G issued through the Science Mission Directorate Near-Earth Objects Observations Program. The CRTS survey is supported by the U.S. National Science Foundation under grants AST-0909182.

References

- Andronov I. L. 1994, *Odessa Astronomical Publications*, **7**, 49, [1994OAP.....7...49A](#)
- Andronov I. L. 2020, *Knowledge Discovery in Big Data from Astronomy and Earth Observation*, 1st Edition. Edited by P. Škoda and F. Adam. ISBN: 978-0-128-19154-5. Elsevier, 2020, p.191, [2020kdbd.book..191A](#)
- Andronov, I. L., & Baklanov, A. V. 2004 *Astronomical School's Report*, **5**, 264 [2004AstSR...5..264A](#)
- Andrych, K. D., Andronov, I. L., Chinarova, L. L., & Marsakova, V. I. 2015, *Odessa Astronomical Publications*, **28**, 158, [2015OAP....28..158A](#)

Andrych, K. D., Andronov, I. L., & Chinarova, L. L. 2020, *Journal of Physical Studies*, **24**, 1902, [2020JPhSt..24.1902A](#)

Axelsen, R. A., & Napier-Munn, T. 2020, *JAAVSO*, **48**, 241, [2020JAVSO..48..241A](#)

Baglin, A., Breger, M., Chevalier, C. et al. 1973, *A&A*, **23**, 221, [1973A&A....23..221B](#)

Benn D., 2012, *JAAVSO*, **40**, 852, [2012JAVSO..40..852B](#)

Benn, D., Beck, S., Pyatnytskyy, M. et al. 2024, <https://github.com/AAVSO/VStar>

Breger, M. 2000a, *Baltic Astronomy*, **9**, 149, [2000BaltA...9..149B](#)

Breger, M. 2000b, *ASP Conference Series*, **210**, 3, [2000ASPC..210....3B](#)

Butters, O. W., West, R. G., Anderson, D. R. et al. 2010, *A&A*, **520**, L10, [2010A&A...520L..10B](#)

Collins, K. A., Kielkopf, J. F., Stassun, K. G., and Hessman, F. V. 2017, *AJ*, **153**, 77, [2017AJ....153..77C](#)

Drake, A. J., Djorgovski, S. G., Mahabal, A. et al. 2009, *ApJ*, **696**, 870, [2009ApJ...696..870D](#)

Gaia Collaboration 2022, *VizieR Online Data Catalog: Gaia DR3 Part 1. Main source*, [2022yCat.1355....0G](#)

Gaia Collaboration 2023, *A&A*, **674**, id.A1, [2023A&A...674A...1G](#)

Gajdoš, P., & Parimucha, Š. 2019, *Astrophysics Source Code Library*, record ascl:1901.002, [2019ascl.soft01002G](#)

Gajdoš, P. 2023, *OEJV*, **241**, 1, [2023OEJV..241....1G](#)

Handler, G. 2009, *AIP Conference Proceedings*, **1170**, 403, [2009AIPC.1170..403H](#)

Henden, A. A., Levine, S., Terrell, D., Welch, D. L., Munari, U., Kloppenborg, B. K. 2018, *American Astronomical Society, AAS Meeting #232*, id. 223.06 [2018AAS..23222306H](#)

Kochanek, C. S., Shappee, B. J., Stanek, K. Z. et al. 2017, *PASP*, **129**, 104502, [2017PASP..129j4502K](#)

Laney, C. D., Joner, M., & Rodriguez, E. 2003, *ASP Conference Series*, **292**, 203, [2003ASPC..292..203L](#)

Lightkurve Collaboration, Cardoso, J. V. d. M., Hedges, C. et al. 2018, *Astrophysics Source Code Library*, record ascl:1812.013, [2018ascl.soft12013L](#)

Masci, F. J., Laher, R. R., Rusholme, B. et al. 2019, *PASP*, **131**, 018003, [2019PASP..131a8003M](#)

McNamara, D. 1997, *PASP*, **109**, 1221, [1997PASP..109.1221M](#)

McNamara, D. H., Madsen, J. B., Barnes, J., Erickson, B. F. 2000, *PASP*, **112**, 202,
[2000PASP..112..202M](#)

McNamara, D. H. 2011, *AJ*, **142**, 110, [2011AJ....142..110M](#)

Pyatnytsky, M. 2021, *JAAVSO*, **49**, 58, [2021JAVSO..49...58P](#)

Pyatnytsky, M. Yu., & Andronov, I. L. 2024, *RNAAS*, **8**, 159 [2024RNAAS...8..159P](#)

Ricker, G. R., Winn, J. N., Vanderspek, R. et al. 2014, *Proceedings of the SPIE*, **9143**,
 914320, [2014SPIE.9143E..20R](#)

Stassun, K. G., Oelkers, R. J., Paegert, M. et al. 2019, *AJ*, **158**, 138, [2019AJ....158..138S](#)

Sterken C., ed. 2005, *ASP Conference Series*, **335**, [2005ASPC..335.....S](#)

Watson, C. L., Henden, A. A., Price, A. 2006, The Society for Astronomical Sciences
 25th Annual Symposium on Telescope Science. Held May 23-25, 2006, at Big Bear, CA.
 Published by the Society for Astronomical Sciences, p. 47 [2006SASS...25...47W](#)

Xue, W., Niu, J.-S., Xue, H.-F., Yin, S. 2023, *Research in Astronomy and Astrophysics*,
23, id.075002, [2023RAA....23g5002X](#)

Ziaali, E., Bedding, T. R., Murphy, S. J. et al. 2019, *MNRAS*, **486**, 4348,
[2019MNRAS.486.4348Z](#)

Table 3: Times of maxima and $O - C$ values calculated
 for the period and initial epoch specified in Tab. 2.

BJD_{TDB} -2400000	Error [d]	Epoch [cycle number]	$O - C$ [d]	Half of the folding interval [d]	Source	Filter
53138.4348	0.0026	-94783	-0.0248	8	SuperWASP	Clear
54154.4671	0.0033	-79933	-0.0161	71	SuperWASP	Clear
53952.3556	0.0013	-82887	-0.0175	279	CRTS	Clear
54694.8459	0.0020	-72035	-0.0113	304	CRTS	Clear
55418.8621	0.0015	-61453	-0.0059	300	CRTS	Clear
56159.3660	0.0013	-50630	-0.0019	294	CRTS	Clear
58180.7412	0.0020	-21086	-0.0003	117	ASAS-SN	g
58546.0991	0.0020	-15746	-0.0004	128	ASAS-SN	g
58906.6679	0.0019	-10476	-0.0002	129	ASAS-SN	g
59268.2624	0.0022	-5191	-0.0007	137	ASAS-SN	g
59634.2365	0.0027	158	-0.0003	135	ASAS-SN	g
59998.7743	0.0030	5486	0.0007	136	ASAS-SN	g
60365.2948	0.0017	10843	0.0001	134	ASAS-SN	g
56701.9307	0.0016	-42700	-0.0006	126	ASAS-SN	V

57060.4472	0.0015	-37460	-0.0001	122	ASAS-SN	V
57429.9788	0.0014	-32059	-0.0001	116	ASAS-SN	V
57807.3098	0.0015	-26544	-0.0003	130	ASAS-SN	V
58251.0768	0.0017	-20058	0.0005	197	ASAS-SN	V
58546.3734	0.0011	-15742	0.0003	116	ZTF	g
58895.3789	0.0008	-10641	0.0000	118	ZTF	g
59254.3742	0.0010	-5394	0.0002	113	ZTF	g
59625.4109	0.0013	29	0.0002	115	ZTF	g
59998.2950	0.0014	5479	0.0003	118	ZTF	g
60357.8377	0.0011	10734	0.0007	107	ZTF	g
58544.8689	0.0013	-15764	0.0010	118	ZTF	r
58899.3471	0.0016	-10583	-0.0001	137	ZTF	r
59266.8265	0.0018	-5212	0.0002	137	ZTF	r
59613.8482	0.0019	-140	0.0003	125	ZTF	r
59986.3899	0.0020	5305	0.0001	130	ZTF	r
60341.8275	0.0022	10500	0.0005	121	ZTF	r
59623.4265	0.0015	0	-0.0001	n.a.	PMAK	V
59624.3840	0.0015	14	-0.0004	n.a.	PMAK	V
59629.3107	0.0020	86	0.0001	n.a.	PMAK	V
59629.4475	0.0012	88	0.0000	n.a.	PMAK	V
60262.3241	0.0012	9338	0.0001	n.a.	TESS	TESS
60262.3925	0.0010	9339	0.0000	n.a.	TESS	TESS
60262.4605	0.0007	9340	-0.0003	n.a.	TESS	TESS
60262.5293	0.0014	9341	0.0000	n.a.	TESS	TESS
60262.5976	0.0007	9342	0.0000	n.a.	TESS	TESS
60262.6663	0.0012	9343	0.0002	n.a.	TESS	TESS
60262.7344	0.0013	9344	-0.0002	n.a.	TESS	TESS
60262.8025	0.0012	9345	-0.0004	n.a.	TESS	TESS
60262.8716	0.0008	9346	0.0002	n.a.	TESS	TESS
60262.9396	0.0010	9347	-0.0002	n.a.	TESS	TESS
60263.0086	0.0012	9348	0.0004	n.a.	TESS	TESS
60263.0773	0.0009	9349	0.0007	n.a.	TESS	TESS
60263.1451	0.0008	9350	0.0001	n.a.	TESS	TESS
60263.2134	0.0010	9351	-0.0001	n.a.	TESS	TESS
60263.2820	0.0011	9352	0.0001	n.a.	TESS	TESS
60263.3507	0.0007	9353	0.0004	n.a.	TESS	TESS
60263.4184	0.0016	9354	-0.0004	n.a.	TESS	TESS
60263.4868	0.0005	9355	-0.0003	n.a.	TESS	TESS
60263.5554	0.0007	9356	-0.0002	n.a.	TESS	TESS
60263.6240	0.0013	9357	0.0001	n.a.	TESS	TESS

60263.6918	0.0011	9358	-0.0006	n.a.	TESS	TESS
60263.7609	0.0008	9359	0.0000	n.a.	TESS	TESS
60263.8289	0.0017	9360	-0.0003	n.a.	TESS	TESS
60263.8976	0.0011	9361	0.0000	n.a.	TESS	TESS
60263.9661	0.0008	9362	0.0000	n.a.	TESS	TESS
60264.0348	0.0014	9363	0.0003	n.a.	TESS	TESS
60264.1028	0.0005	9364	-0.0001	n.a.	TESS	TESS
60264.1713	0.0006	9365	-0.0001	n.a.	TESS	TESS
60264.2403	0.0010	9366	0.0005	n.a.	TESS	TESS
60264.3076	0.0009	9367	-0.0005	n.a.	TESS	TESS
60264.3764	0.0013	9368	-0.0001	n.a.	TESS	TESS
60264.4450	0.0013	9369	0.0000	n.a.	TESS	TESS
60264.5133	0.0009	9370	-0.0001	n.a.	TESS	TESS
60264.5816	0.0008	9371	-0.0003	n.a.	TESS	TESS
60264.6503	0.0015	9372	0.0001	n.a.	TESS	TESS
60264.7188	0.0012	9373	0.0001	n.a.	TESS	TESS
60264.7872	0.0010	9374	0.0001	n.a.	TESS	TESS
60264.8552	0.0010	9375	-0.0003	n.a.	TESS	TESS
60264.9243	0.0011	9376	0.0004	n.a.	TESS	TESS
60264.9922	0.0007	9377	-0.0002	n.a.	TESS	TESS
60265.0610	0.0008	9378	0.0002	n.a.	TESS	TESS
60265.1292	0.0007	9379	0.0000	n.a.	TESS	TESS
60265.1977	0.0012	9380	0.0000	n.a.	TESS	TESS
60265.2663	0.0012	9381	0.0002	n.a.	TESS	TESS
60265.3341	0.0013	9382	-0.0004	n.a.	TESS	TESS
60265.4029	0.0007	9383	0.0000	n.a.	TESS	TESS
60265.4711	0.0008	9384	-0.0002	n.a.	TESS	TESS
60265.5392	0.0010	9385	-0.0005	n.a.	TESS	TESS
60265.6078	0.0008	9386	-0.0004	n.a.	TESS	TESS
60265.6761	0.0009	9387	-0.0005	n.a.	TESS	TESS
60265.7450	0.0011	9388	0.0000	n.a.	TESS	TESS
60265.8135	0.0008	9389	0.0001	n.a.	TESS	TESS
60265.8817	0.0007	9390	-0.0002	n.a.	TESS	TESS
60265.9501	0.0009	9391	-0.0001	n.a.	TESS	TESS
60266.0185	0.0011	9392	-0.0002	n.a.	TESS	TESS
60266.0868	0.0012	9393	-0.0003	n.a.	TESS	TESS
60266.1552	0.0008	9394	-0.0003	n.a.	TESS	TESS
60266.2238	0.0010	9395	-0.0001	n.a.	TESS	TESS
60266.2926	0.0010	9396	0.0003	n.a.	TESS	TESS
60266.6347	0.0007	9401	0.0003	n.a.	TESS	TESS

60266.7027	0.0007	9402	-0.0001	n.a.	TESS	TESS
60266.7713	0.0012	9403	0.0000	n.a.	TESS	TESS
60266.8399	0.0012	9404	0.0002	n.a.	TESS	TESS
60266.9077	0.0009	9405	-0.0003	n.a.	TESS	TESS
60266.9764	0.0011	9406	-0.0002	n.a.	TESS	TESS
60267.0449	0.0008	9407	0.0000	n.a.	TESS	TESS
60267.1130	0.0008	9408	-0.0003	n.a.	TESS	TESS
60267.1821	0.0007	9409	0.0003	n.a.	TESS	TESS
60267.2501	0.0008	9410	-0.0001	n.a.	TESS	TESS
60267.3186	0.0010	9411	0.0000	n.a.	TESS	TESS
60267.3872	0.0014	9412	0.0002	n.a.	TESS	TESS
60267.4550	0.0010	9413	-0.0005	n.a.	TESS	TESS
60267.5238	0.0009	9414	0.0000	n.a.	TESS	TESS
60267.5920	0.0014	9415	-0.0003	n.a.	TESS	TESS
60267.6607	0.0006	9416	0.0000	n.a.	TESS	TESS
60267.7289	0.0006	9417	-0.0002	n.a.	TESS	TESS
60267.7975	0.0005	9418	-0.0001	n.a.	TESS	TESS
60267.8664	0.0010	9419	0.0005	n.a.	TESS	TESS
60267.9343	0.0010	9420	-0.0001	n.a.	TESS	TESS
60268.0026	0.0012	9421	-0.0002	n.a.	TESS	TESS
60268.0711	0.0008	9422	-0.0002	n.a.	TESS	TESS
60268.1397	0.0009	9423	0.0000	n.a.	TESS	TESS
60268.2078	0.0004	9424	-0.0003	n.a.	TESS	TESS
60268.2762	0.0008	9425	-0.0003	n.a.	TESS	TESS
60268.3452	0.0005	9426	0.0003	n.a.	TESS	TESS
60268.4134	0.0011	9427	0.0001	n.a.	TESS	TESS
60268.4821	0.0010	9428	0.0003	n.a.	TESS	TESS
60268.5501	0.0007	9429	-0.0001	n.a.	TESS	TESS
60268.6183	0.0013	9430	-0.0003	n.a.	TESS	TESS
60268.6872	0.0008	9431	0.0002	n.a.	TESS	TESS
60268.7560	0.0010	9432	0.0006	n.a.	TESS	TESS
60268.8238	0.0007	9433	0.0000	n.a.	TESS	TESS
60268.8924	0.0010	9434	0.0002	n.a.	TESS	TESS
60268.9608	0.0009	9435	0.0001	n.a.	TESS	TESS
60269.0293	0.0015	9436	0.0002	n.a.	TESS	TESS
60269.0977	0.0007	9437	0.0002	n.a.	TESS	TESS
60269.1657	0.0008	9438	-0.0002	n.a.	TESS	TESS
60269.2346	0.0008	9439	0.0002	n.a.	TESS	TESS
60269.3030	0.0007	9440	0.0002	n.a.	TESS	TESS
60269.3713	0.0012	9441	0.0001	n.a.	TESS	TESS

60269.4395	0.0010	9442	-0.0001	n.a.	TESS	TESS
60269.5081	0.0008	9443	0.0001	n.a.	TESS	TESS
60269.5765	0.0013	9444	0.0000	n.a.	TESS	TESS
60269.6450	0.0011	9445	0.0001	n.a.	TESS	TESS
60269.7136	0.0018	9446	0.0004	n.a.	TESS	TESS
60269.7816	0.0004	9447	-0.0001	n.a.	TESS	TESS
60269.8500	0.0005	9448	-0.0002	n.a.	TESS	TESS
60269.9189	0.0008	9449	0.0004	n.a.	TESS	TESS
60269.9872	0.0009	9450	0.0003	n.a.	TESS	TESS
60270.0560	0.0010	9451	0.0006	n.a.	TESS	TESS
60270.1240	0.0013	9452	0.0002	n.a.	TESS	TESS
60270.1922	0.0006	9453	0.0000	n.a.	TESS	TESS
60270.2609	0.0006	9454	0.0003	n.a.	TESS	TESS
60270.3288	0.0011	9455	-0.0003	n.a.	TESS	TESS
60270.3977	0.0010	9456	0.0002	n.a.	TESS	TESS
60270.4660	0.0006	9457	0.0001	n.a.	TESS	TESS
60270.5344	0.0007	9458	0.0001	n.a.	TESS	TESS
60270.6025	0.0010	9459	-0.0002	n.a.	TESS	TESS
60270.6710	0.0007	9460	-0.0001	n.a.	TESS	TESS
60270.7393	0.0010	9461	-0.0003	n.a.	TESS	TESS
60270.8080	0.0008	9462	0.0000	n.a.	TESS	TESS
60270.8767	0.0012	9463	0.0003	n.a.	TESS	TESS
60270.9446	0.0010	9464	-0.0002	n.a.	TESS	TESS
60271.0134	0.0007	9465	0.0001	n.a.	TESS	TESS
60271.0819	0.0007	9466	0.0002	n.a.	TESS	TESS
60271.1503	0.0010	9467	0.0002	n.a.	TESS	TESS
60271.2186	0.0005	9468	0.0001	n.a.	TESS	TESS
60271.2868	0.0006	9469	-0.0001	n.a.	TESS	TESS
60271.3553	0.0009	9470	-0.0001	n.a.	TESS	TESS
60271.4235	0.0006	9471	-0.0002	n.a.	TESS	TESS
60271.4918	0.0016	9472	-0.0003	n.a.	TESS	TESS
60271.5606	0.0008	9473	0.0000	n.a.	TESS	TESS
60271.6286	0.0006	9474	-0.0004	n.a.	TESS	TESS
60271.6972	0.0006	9475	-0.0002	n.a.	TESS	TESS
60271.7661	0.0004	9476	0.0002	n.a.	TESS	TESS
60271.8342	0.0008	9477	-0.0001	n.a.	TESS	TESS
60271.9026	0.0011	9478	-0.0001	n.a.	TESS	TESS
60271.9712	0.0011	9479	0.0001	n.a.	TESS	TESS
60272.0394	0.0009	9480	-0.0001	n.a.	TESS	TESS
60272.1076	0.0012	9481	-0.0004	n.a.	TESS	TESS

60272.1760	0.0006	9482	-0.0004	n.a.	TESS	TESS
60272.2450	0.0009	9483	0.0002	n.a.	TESS	TESS
60272.3129	0.0010	9484	-0.0003	n.a.	TESS	TESS
60272.3814	0.0007	9485	-0.0002	n.a.	TESS	TESS
60272.4497	0.0007	9486	-0.0003	n.a.	TESS	TESS
60272.5185	0.0009	9487	0.0001	n.a.	TESS	TESS
60272.5868	0.0012	9488	0.0000	n.a.	TESS	TESS
60272.6551	0.0009	9489	-0.0002	n.a.	TESS	TESS
60272.7237	0.0010	9490	-0.0001	n.a.	TESS	TESS
60272.7922	0.0010	9491	0.0000	n.a.	TESS	TESS
60272.8607	0.0012	9492	0.0001	n.a.	TESS	TESS
60272.9291	0.0015	9493	0.0001	n.a.	TESS	TESS
60275.8709	0.0017	9536	-0.0001	n.a.	TESS	TESS
60275.9392	0.0008	9537	-0.0003	n.a.	TESS	TESS
60276.0080	0.0010	9538	0.0001	n.a.	TESS	TESS
60276.0762	0.0007	9539	0.0000	n.a.	TESS	TESS
60276.1448	0.0008	9540	0.0001	n.a.	TESS	TESS
60276.2131	0.0016	9541	0.0000	n.a.	TESS	TESS
60276.2816	0.0009	9542	0.0000	n.a.	TESS	TESS
60276.3502	0.0011	9543	0.0003	n.a.	TESS	TESS
60276.4184	0.0011	9544	0.0001	n.a.	TESS	TESS
60276.4868	0.0015	9545	0.0000	n.a.	TESS	TESS
60276.5554	0.0012	9546	0.0002	n.a.	TESS	TESS
60276.6235	0.0008	9547	-0.0001	n.a.	TESS	TESS
60276.6922	0.0009	9548	0.0001	n.a.	TESS	TESS
60276.7606	0.0005	9549	0.0002	n.a.	TESS	TESS
60276.8289	0.0008	9550	0.0000	n.a.	TESS	TESS
60276.8973	0.0009	9551	0.0000	n.a.	TESS	TESS
60276.9657	0.0008	9552	0.0000	n.a.	TESS	TESS
60277.0344	0.0009	9553	0.0003	n.a.	TESS	TESS
60277.1026	0.0011	9554	0.0001	n.a.	TESS	TESS
60277.1708	0.0009	9555	-0.0001	n.a.	TESS	TESS
60277.2395	0.0007	9556	0.0001	n.a.	TESS	TESS
60277.3076	0.0010	9557	-0.0002	n.a.	TESS	TESS
60277.3759	0.0007	9558	-0.0003	n.a.	TESS	TESS
60277.4448	0.0012	9559	0.0002	n.a.	TESS	TESS
60277.5128	0.0008	9560	-0.0003	n.a.	TESS	TESS
60277.5820	0.0009	9561	0.0005	n.a.	TESS	TESS
60277.6498	0.0005	9562	-0.0001	n.a.	TESS	TESS
60277.7188	0.0007	9563	0.0005	n.a.	TESS	TESS

60277.7864	0.0007	9564	-0.0003	n.a.	TESS	TESS
60277.8550	0.0007	9565	-0.0002	n.a.	TESS	TESS
60277.9238	0.0008	9566	0.0002	n.a.	TESS	TESS
60277.9918	0.0011	9567	-0.0001	n.a.	TESS	TESS
60278.0605	0.0010	9568	0.0000	n.a.	TESS	TESS
60278.1290	0.0014	9569	0.0001	n.a.	TESS	TESS
60278.1970	0.0008	9570	-0.0003	n.a.	TESS	TESS
60278.2656	0.0008	9571	-0.0001	n.a.	TESS	TESS
60278.3339	0.0009	9572	-0.0002	n.a.	TESS	TESS
60278.4025	0.0005	9573	0.0000	n.a.	TESS	TESS
60278.4708	0.0011	9574	-0.0001	n.a.	TESS	TESS
60278.5395	0.0009	9575	0.0001	n.a.	TESS	TESS
60278.6079	0.0007	9576	0.0001	n.a.	TESS	TESS
60278.6762	0.0013	9577	0.0000	n.a.	TESS	TESS
60278.7447	0.0010	9578	0.0001	n.a.	TESS	TESS
60278.8124	0.0009	9579	-0.0006	n.a.	TESS	TESS
60278.8813	0.0008	9580	-0.0001	n.a.	TESS	TESS
60278.9496	0.0006	9581	-0.0002	n.a.	TESS	TESS
60279.0182	0.0010	9582	0.0000	n.a.	TESS	TESS
60279.0866	0.0008	9583	-0.0001	n.a.	TESS	TESS
60279.1555	0.0008	9584	0.0004	n.a.	TESS	TESS
60279.2238	0.0008	9585	0.0003	n.a.	TESS	TESS
60279.2918	0.0010	9586	-0.0001	n.a.	TESS	TESS
60279.5653	0.0009	9590	-0.0003	n.a.	TESS	TESS
60279.6342	0.0010	9591	0.0002	n.a.	TESS	TESS
60279.7024	0.0011	9592	-0.0001	n.a.	TESS	TESS
60279.7708	0.0004	9593	-0.0001	n.a.	TESS	TESS
60279.8395	0.0010	9594	0.0002	n.a.	TESS	TESS
60279.9075	0.0004	9595	-0.0002	n.a.	TESS	TESS
60279.9761	0.0009	9596	0.0000	n.a.	TESS	TESS
60280.0448	0.0006	9597	0.0002	n.a.	TESS	TESS
60280.1130	0.0008	9598	0.0000	n.a.	TESS	TESS
60280.1815	0.0005	9599	0.0001	n.a.	TESS	TESS
60280.2500	0.0005	9600	0.0002	n.a.	TESS	TESS
60280.3186	0.0007	9601	0.0003	n.a.	TESS	TESS
60280.3866	0.0008	9602	-0.0001	n.a.	TESS	TESS
60280.4552	0.0010	9603	0.0001	n.a.	TESS	TESS
60280.5239	0.0005	9604	0.0004	n.a.	TESS	TESS
60280.5920	0.0007	9605	0.0001	n.a.	TESS	TESS
60280.6604	0.0005	9606	0.0001	n.a.	TESS	TESS

60280.7284	0.0011	9607	-0.0004	n.a.	TESS	TESS
60280.7969	0.0013	9608	-0.0003	n.a.	TESS	TESS
60280.8656	0.0010	9609	0.0000	n.a.	TESS	TESS
60280.9344	0.0012	9610	0.0004	n.a.	TESS	TESS
60281.0025	0.0010	9611	0.0001	n.a.	TESS	TESS
60281.0708	0.0011	9612	-0.0001	n.a.	TESS	TESS
60281.1390	0.0007	9613	-0.0003	n.a.	TESS	TESS
60281.2075	0.0012	9614	-0.0002	n.a.	TESS	TESS
60281.2761	0.0005	9615	0.0000	n.a.	TESS	TESS
60281.3445	0.0009	9616	-0.0001	n.a.	TESS	TESS
60281.4127	0.0007	9617	-0.0002	n.a.	TESS	TESS
60281.4816	0.0008	9618	0.0002	n.a.	TESS	TESS
60281.5496	0.0010	9619	-0.0001	n.a.	TESS	TESS
60281.6182	0.0010	9620	0.0000	n.a.	TESS	TESS
60281.6867	0.0009	9621	0.0000	n.a.	TESS	TESS
60281.7554	0.0009	9622	0.0003	n.a.	TESS	TESS
60281.8236	0.0007	9623	0.0001	n.a.	TESS	TESS
60281.8917	0.0012	9624	-0.0001	n.a.	TESS	TESS
60281.9600	0.0007	9625	-0.0003	n.a.	TESS	TESS
60282.0290	0.0011	9626	0.0003	n.a.	TESS	TESS
60282.0970	0.0007	9627	-0.0001	n.a.	TESS	TESS
60282.1654	0.0007	9628	-0.0002	n.a.	TESS	TESS
60282.2338	0.0009	9629	-0.0002	n.a.	TESS	TESS
60282.3027	0.0012	9630	0.0003	n.a.	TESS	TESS
60282.3709	0.0008	9631	0.0001	n.a.	TESS	TESS
60282.4391	0.0005	9632	-0.0001	n.a.	TESS	TESS
60282.5076	0.0006	9633	0.0000	n.a.	TESS	TESS
60282.5761	0.0008	9634	0.0000	n.a.	TESS	TESS
60282.6444	0.0004	9635	-0.0001	n.a.	TESS	TESS
60282.7128	0.0010	9636	-0.0001	n.a.	TESS	TESS
60282.7821	0.0007	9637	0.0008	n.a.	TESS	TESS
60282.8494	0.0008	9638	-0.0004	n.a.	TESS	TESS
60282.9183	0.0009	9639	0.0001	n.a.	TESS	TESS
60282.9868	0.0007	9640	0.0002	n.a.	TESS	TESS
60283.0548	0.0010	9641	-0.0002	n.a.	TESS	TESS
60283.1233	0.0009	9642	-0.0001	n.a.	TESS	TESS
60283.1920	0.0008	9643	0.0002	n.a.	TESS	TESS
60283.2602	0.0011	9644	0.0000	n.a.	TESS	TESS
60283.3288	0.0009	9645	0.0001	n.a.	TESS	TESS
60283.3969	0.0011	9646	-0.0002	n.a.	TESS	TESS

60283.4653	0.0011	9647	-0.0002	n.a.	TESS	TESS
60283.5340	0.0011	9648	0.0000	n.a.	TESS	TESS
60283.6027	0.0008	9649	0.0003	n.a.	TESS	TESS
60283.6706	0.0009	9650	-0.0002	n.a.	TESS	TESS
60283.7392	0.0007	9651	0.0000	n.a.	TESS	TESS
60283.8075	0.0011	9652	-0.0001	n.a.	TESS	TESS
60283.8758	0.0007	9653	-0.0003	n.a.	TESS	TESS
60283.9443	0.0011	9654	-0.0002	n.a.	TESS	TESS
60284.0132	0.0009	9655	0.0004	n.a.	TESS	TESS
60284.0809	0.0010	9656	-0.0004	n.a.	TESS	TESS
60284.1499	0.0014	9657	0.0002	n.a.	TESS	TESS
60284.2178	0.0007	9658	-0.0003	n.a.	TESS	TESS
60284.2865	0.0011	9659	-0.0001	n.a.	TESS	TESS
60284.3550	0.0014	9660	0.0000	n.a.	TESS	TESS
60284.4240	0.0008	9661	0.0006	n.a.	TESS	TESS
60284.4919	0.0007	9662	0.0001	n.a.	TESS	TESS
60284.5603	0.0004	9663	0.0000	n.a.	TESS	TESS
60284.6286	0.0006	9664	-0.0001	n.a.	TESS	TESS
60284.6968	0.0009	9665	-0.0003	n.a.	TESS	TESS
60284.7656	0.0015	9666	0.0002	n.a.	TESS	TESS
60284.8341	0.0009	9667	0.0002	n.a.	TESS	TESS
60284.9022	0.0010	9668	-0.0001	n.a.	TESS	TESS
60284.9710	0.0014	9669	0.0003	n.a.	TESS	TESS
60285.0392	0.0011	9670	0.0000	n.a.	TESS	TESS
60285.1076	0.0013	9671	0.0000	n.a.	TESS	TESS
60285.1758	0.0008	9672	-0.0002	n.a.	TESS	TESS
60285.2446	0.0011	9673	0.0001	n.a.	TESS	TESS
60285.3129	0.0011	9674	0.0001	n.a.	TESS	TESS
60285.3812	0.0006	9675	-0.0001	n.a.	TESS	TESS
60285.4496	0.0010	9676	-0.0001	n.a.	TESS	TESS
60285.5179	0.0012	9677	-0.0002	n.a.	TESS	TESS